CELL BIOLOGY

Nuclear receptors FXR and SHP regulate protein N-glycan modifications in the liver

Bhoomika Mathur[1], Asif Shajahan[2], Waqar Arif[3], Qiushi Chen[2], Nicholas J. Hand[4], Lara K. Abramowitz[5], Kristina Schoonjans[6], Daniel J. Rader[4], Auinash Kalsotra[3], John A. Hanover[5], Parastoo Azadi[2], Sayeepriyadarshini Anakk[1,7]*

Nuclear receptors farnesoid X receptor (FXR) and small heterodimer partner (SHP) are key regulators of metabolism. Here, we report a previously unknown function for the hepatic FXR-SHP axis in controlling protein N-linked glycosylation. Transcriptome analysis in liver-specific Fxr-Shp double knockout (LDKO) livers revealed induction of genes encoding enzymes in the N-glycosylation pathway, including *Mgat5*, *Fut8*, *St3gal6*, and *St6gal1*. FXR activation suppressed *Mgat5*, while Shp deletion induced *St3gal6* and *St6gal1*. Increased percentages of core-fucosylated and triantennary glycan moieties were seen in LDKO livers, and proteins with the "hyperglycoforms" preferentially localized to exosomes and lysosomes. This up-regulation of N-glycosylation machinery was specific to the Golgi apparatus and not the endoplasmic reticulum. The increased glycan complexity in the LDKO correlated well with dilated unstacked Golgi ribbons and alterations in the secretion of albumin, cholesterol, and triglycerides. Our findings demonstrate a role for the FXR-SHP axis in maintaining glycoprotein diversity in the liver.

INTRODUCTION

N-Glycosylation is a key posttranslational modification that decides the fate of several liver proteins, including their targeting to the plasma membrane or for secretion. Briefly, various combinations of sugar molecules (glycan moieties) attach covalently to the nitrogen of asparagine residues of a protein (*1*, *2*), including mannose and glucose in the endoplasmic reticulum (ER) lumen (*3*–*6*). Further glycan processing occurs in cis- and medial-Golgi, including the addition of GlcNAc (*N*-acetylglucosamine) by the MGAT (Mannosyl-glycoprotein *N*-acetylglucosaminyltransferase) family of proteins resulting in "antennae" (or branch) glycan moieties. These branched glycans are finally modified in trans-Golgi via the addition of fucose by fucosyltransferase (*Futs*), *N*-acetylgalactosamine by GalNAc transferases, and sialic acid by sialyltransferases (*Stgals* and *Stsias*) (*5*, *7*, *8*). These complex glycan structures not only allow for structural and functional heterogeneity in the tissue glycoproteome but also are important for maintaining appropriate liver function (*9*–*11*). However, the regulation of this essential protein modification in the liver remains understudied.

Farnesoid X receptor (FXR; NR1H4) and small heterodimer partner (SHP; NR0B2) belong to a superfamily of nuclear receptors that regulate transcription of several genes involved in intermediary metabolism. Global deletion of FXR and SHP induces liver injury (*12*) and ultimately results in spontaneous hepatic carcinogenesis in mice (*13*). Here, we set out to identify molecular networks coordinated by hepatic FXR and SHP, in addition to their conventional metabolic targets. Using high-throughput RNA sequencing (RNA-seq), glycomics, glycoproteomics analyses, and electron microscopy, we found a key role for this axis in regulating the liver *N*-glycome.

[1]Department of Molecular and Integrative Physiology, University of Illinois at Urbana-Champaign, Urbana, IL, USA. [2]Complex Carbohydrate Research Center, University of Georgia, Athens, GA, USA. [3]Department of Biochemistry, University of Illinois at Urbana-Champaign, Urbana, IL, USA. [4]Perelman School of Medicine, University of Pennsylvania, Philadelphia, PA, USA. [5]Laboratory of Cell and Molecular Biology, National Institute of Diabetes and Digestive and Kidney Diseases, National Institutes of Health, Bethesda, MD, USA. [6]École polytechnique fédérale de Lausanne, 1015 Lausanne, Switzerland. [7]Cancer Center at Illinois, University of Illinois at Urbana-Champaign, Urbana, IL, USA.
*Corresponding author. Email: anakk@illinois.edu

RESULTS

Liver-specific Fxr-Shp double-knockout mice exhibit defective bile acid response

We generated liver-specific *Fxr-Shp* double-knockout (LDKO) and double-floxed homozygous *Fxr-Shp* (control) mice as shown in fig. S1A. The knockout was validated by genotyping and quantitative reverse transcription polymerase chain reaction (RT-PCR) assays (fig. S1, B and C).

Bile acids (BAs), the cholesterol metabolites synthesized in the liver, are responsible for fat digestion. By activating FXR and SHP in the liver, BAs autoregulate their concentrations (*14*–*17*). LDKO mice exhibited poor response to cholic acid (CA; a primary bile acid in humans) supplemented diet. Focal inflammation and ballooned hepatocytes were observed in chow-fed LDKO livers, which were more evident in CA-fed LDKO livers (fig. S2A). Markers of liver injury, alanine aminotransferase (ALT) and aspartate aminotransferase (AST), were significantly elevated in LDKO + CA (Fig. 1A). Compared to controls, LDKO mice accumulated pathological levels of BAs in the plasma, liver (Fig. 1B), and gall bladder (fig. S2B) in response to the CA diet. However, ileal BA levels were unchanged (fig. S2C), indicating that the intact intestinal FXR-SHP axis in LDKO mice was sufficient to maintain the ileal BA concentrations.

We next investigated whether the genes involved in maintaining BA homeostasis were altered in LDKO mice (fig. S2D). SHP is known to turn off genes responsible for BA synthesis (*14*, *18*–*20*), including *Cyp7a1* (cholesterol 7 alpha-hydroxylase) and *Cyp8b1* (sterol 12-alpha-hydroxylase). Both these genes were poorly repressed in LDKO livers upon CA challenge, unlike the controls. We found that LDKO livers showed reduced basal expression of canalicular transporter *Bsep (Abcb11)* and lost the CA-mediated up-regulation of *Bsep* and *Mdr1a* (*Abcb1a*) expression compared to control livers. Genes responsible for BA uptake into hepatocytes *Ntcp* was up-regulated in LDKO + CA but not in control + CA, whereas *Oatp1* was suppressed in both groups. Although, CA-fed LDKO livers revealed pronounced induction of BA efflux transporters *Mrp3* (*Abcc3*) and *Mrp4* (*Abcc4*) (fig. S2E), it was insufficient to compensate for the loss in canalicular transport, and the increase in hepatic uptake led to excess hepatic BAs.

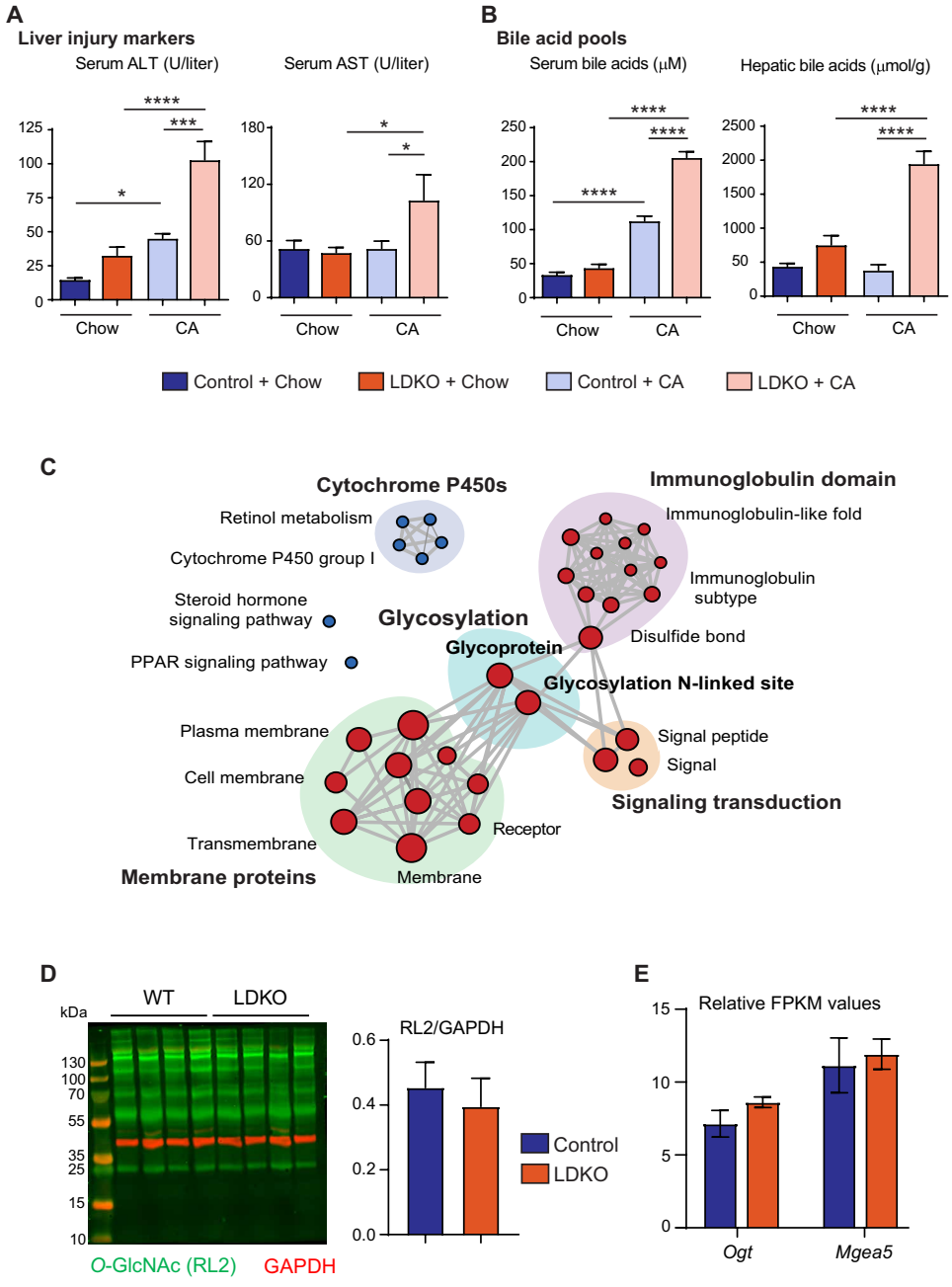

Fig. 1. LDKO mice exhibit a unique induction of N-glycosylation gene machinery. Biochemical characterization revealed (**A**) severe liver injury (marked by serum ALT and AST levels) and (**B**) bile acid accumulation in LDKO + CA mice compared to the controls ($n = 6$ to 11 mice per group, one-way ANOVA, $^{*}P < 0.05$, $^{***}P < 0.001$, and $^{****}P < 0.0001$). (**C**) RNA-seq was performed on the livers of chow-fed control and LDKO mice. Functional clusters display enrichment of glycosylation upon *Fxr-Shp* deletion. Blue circles: down-regulated; red circles: up-regulated in LDKO mice ($n = 3$ mice per group). (**D**) Neither intracellular *O*-GlcNAcylation levels nor (**E**) the genes regulated *O*-GlcNAcylation, *Ogt* and *Mgea5* were enhanced in LDKO mice ($n = 3$ to 4 mice per group; Student *t* test, $P < 0.05$ was considered significant). GAPDH, glyceraldehyde-3-phosphate dehydrogenase. FPKM, fragments per kilobase million; PPAR, peroxisome proliferator–activated receptor.

LDKO mice exhibit increases in N-glycosylation pathway

To decipher the molecular networks coordinately regulated by hepatic FXR-SHP, we performed RNA-seq analysis and found more than 2600 significantly altered transcripts in LDKO livers compared to the controls. Of these, 1253 were up-regulated, while 865 were down-regulated in LDKO livers (fig. S3, A and C). Gene network analysis pinpointed several known signaling and metabolic pathways including response to nutrients, cell adhesion, and drug clearance. Unexpectedly, we found an enrichment of genes involved in the glycosylation pathway (Fig. 1C and fig. S3B). Upon further analysis, we found that these alterations were unique for N-linked, but not O-linked, glycosylation (fig. S3D). Consistent with this observation,

intracellular *O*-GlcNAcylation (Fig. 1D) and the expression of genes regulating *O*-GlcNAcylation, *Ogt*, and *Mgea5* (*21*, *22*) were unchanged (Fig. 1E).

Instead, the RNA-seq data showed up-regulation of essential N-linked glycosyltransferases (*7*, *8*, *23*) (Fig. 2A), such as *Mgat5* (*N*-acetylglucosaminyl-transferase V) that promotes glycan branching, *Fut8* (α-1,6-fucosyltransferase) that adds fucose to the glycan core, and *St3gal6* and *St6gal1* (sialyltransferases) that add sialyl groups (Fig. 2B). These glycosyltransferases "decorate" proteins associated with the cell-matrix and cell-cell contact and promote tumorigenesis (*9*, *24*–*26*). Higher expression of *Mgat5*, *St3gal6*, and *St6gal1* are associated with poor survival of patients with liver cancer (fig. S3E), suggesting that stringent control of their expression is critical to maintain normal liver function.

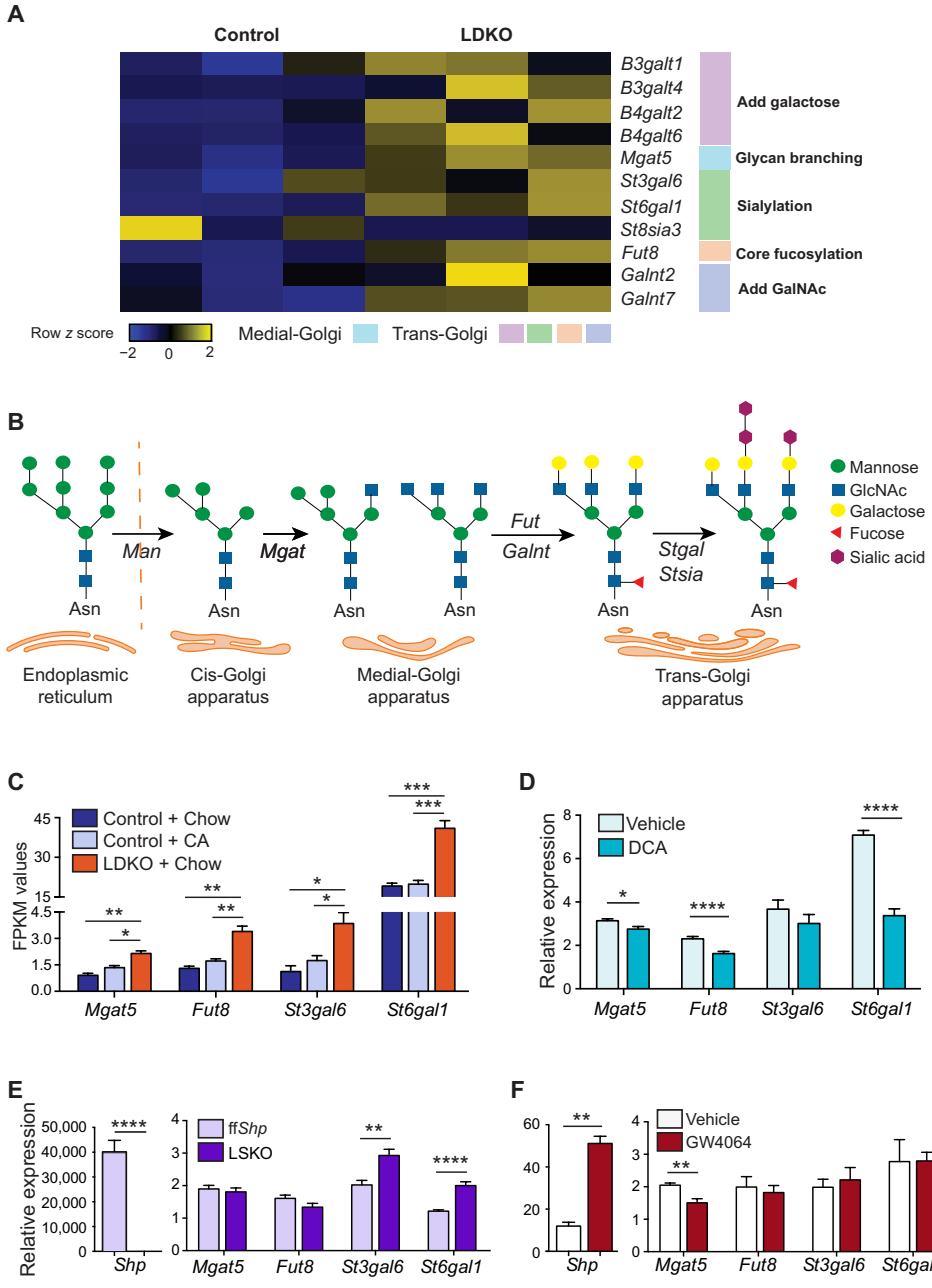

Fig. 2. Up-regulation of N-glycosylation machinery in LDKO livers is dictated by FXR and SHP and not by BA overload. (**A**) Heatmap indicates up-regulation of key glycosyltransferase genes that are involved in "decorating" glycoproteins in LDKO livers. ($n = 3$ mice per group, Student t test, fold change > 1.5, $P < 0.05$). (**B**) Schematic highlighting the steps of cellular protein processing in ER and Golgi apparatus. (**C**) Bar graphs comparing the FPKM values indicate up-regulation of glycosylation genes in LDKO livers is not a consequence of BA overload ($n = 3$ mice per group; one-way ANOVA, $^*P < 0.05$, $^{**}P < 0.01$, and $^{***}P < 0.001$). (**D**) Incubation of primary hepatocytes with a toxic BA, such as DCA, suppresses the N-glycosylation genes instead (n = hepatocytes cultured in triplicates from two mice per group; Student t test, $^*P < 0.05$ and $^{****}P < 0.0001$). Qualitative RT-PCR analysis of (**E**) liver-specific SHP knockout (LSKO) livers and (**F**) FXR-activated (treated with GW4064, FXR agonist) livers reveal that FXR and SHP individually regulate some of these glycosylation genes ($n = 5$ to 8 mice per group; Student t test, $^{**}P < 0.01$ and $^{****}P < 0.0001$).

FXR and SHP, but not BA, overload regulate the induction of *N*-glycosyltransferases

To test whether BA overload seen in the LDKO livers was sufficient to induce expression of N-linked glycosyltransferases, we analyzed the RNA-seq data of CA-treated control livers. We found no significant differences in transcript levels of glycosyltransferases (Fig. 2C). Then, we tested whether a toxic hydrophobic BA, such as deoxycholic acid (DCA), can alter the expression of glycosyltransferases. When we treated primary hepatocytes with DCA, we found a modest suppression in *Mgat5*, *Fut8*, and *St6gal1* expression (Fig. 2D) rather than the induction observed in LDKO livers. These findings demonstrate that elevated BAs are not responsible for the induction of glycosyltransferases.

As global *Fxr-Shp* double-knockout mice show elevated CYP17A1 expression and its enzymatic product 17 hydroxy progesterone (17OHP) (*12*), we investigated and found similar up-regulation of *Cyp17a1* mRNA expression in LDKO livers (fig. S4A). However, serum 17OHP levels in LDKO were below the detectable limit (fig. S4A). Exogenous 17OHP administration to the wild-type (WT) mice (fig. S4, B and C) led to a decrease in mRNA levels of N-glycosylation genes (fig. S4D) with an increase in certain glycan decorations but not fucosylation (fig. S4E). These results indicate that 17OHP is not sufficient to explain the N-glycosylation phenotype of LDKO mice.

Next, we assessed whether *Shp* alone can regulate expression of these genes and found *St3gal6* and *St6gal1* up-regulation in the liver-specific *Shp* knockout mice compared to their respective controls (Fig. 2E). We also tested the role for FXR in controlling the expression of glycosyltransferases by activating it with its agonist GW4064 in WT mice. FXR activation led to a modest but significant down-regulation of *Mgat5* but did not alter the expression of *Fut8*, *St3gal6*, and *St6gal1* levels (Fig. 2F). This result indicates that FXR can suppress *Mgat5* expression, whereas SHP can suppress *Stgal* expression and together coordinate the expression of several glycosyl transferases. We next analyzed the publicly available hepatic chromatin immunoprecipitation sequencing (ChIP-seq) datasets for FXR (*27*) and SHP (*28*) to determine whether these nuclear receptors bind to their respective target genes, *Mgat5*, and *St3gal6* and *St6gal1*. Although no SHP binding was observed in *St3gal6* and *St6gal1* DNA sequences (fig. S5A), we did find a robust FXR-binding peak along with its core motif (ER2, "*TGACCTCAAACTCA*") within the intron 4 of *Mgat5* gene (fig. S5B). These data support the hypothesis that FXR may directly

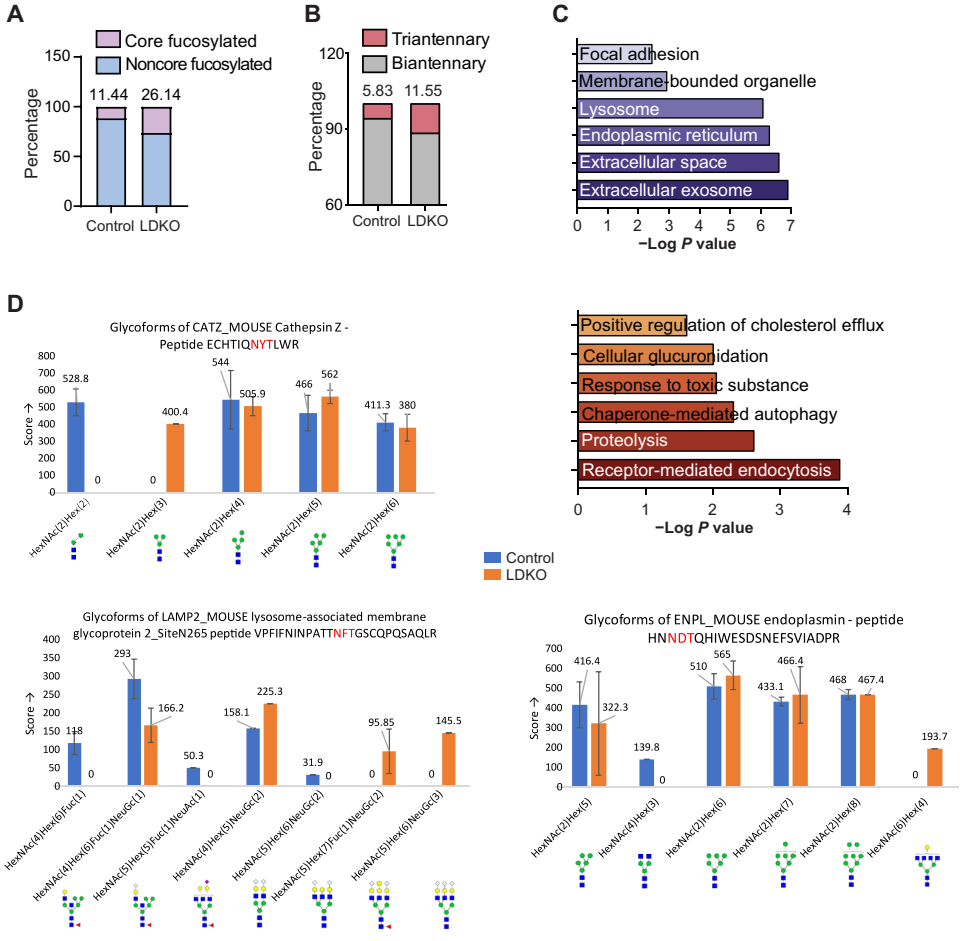

Fig. 3. *Fxr-Shp* ablation results in hyperbranched glycosylations of liver proteins. LDKO liver glycoproteins were isolated and analyzed for their glycan profiles. LDKO livers display increased percentage of (**A**) core fucosylated and (**B**) triantennary glycans in LDKO liver compared to controls ($n = 5$ mice averaged per group). (**C**) Gene Ontology analysis of proteins with increased glycosylation reveals their cellular localization and function ($n = 5$ livers pooled per group). (**D**) Relative ratio of complex, sialylated and fucosylated glycoforms for CATZ, EMPL, and lysosomal membrane protein 2 (LAMP2) indicate enrichment of hyperglycoforms in LDKO livers compared to controls ($n = 5$ mice averaged per group).

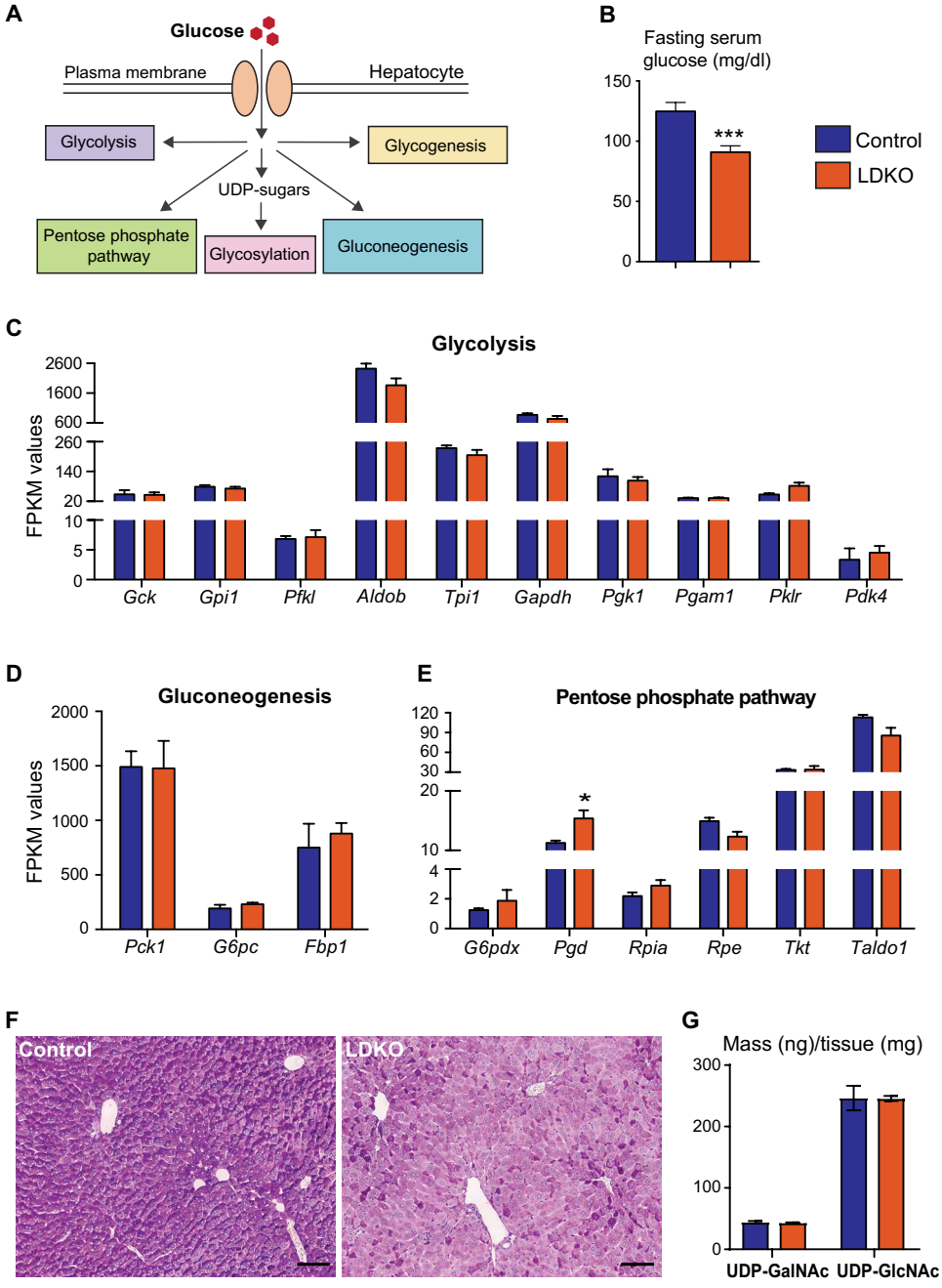

Fig. 4. LDKO livers exhibit any depleted glycogen stores. (**A**) Schematic figure displaying the fate of glucose in a hepatocyte. (**B**) LDKO mice have reduced fasting blood glucose levels ($n = 12$ to 15 mice per group; Student t test, $^{***}P < 0.005$). Bar graphs comparing FPKM values of genes regulating (**C**) glycolysis, (**D**) gluconeogenesis, and (**E**) pentose phosphate pathway show no significant difference between control and LDKO livers ($n = 3$ mice per group; Student t test, $^{*}P < 0.05$). (**F**) PAS staining indicates lower glycogen content in LDKO livers ($n = 5$ mice per group). Scale bars, 50 μm). (**G**) UDP-glycan sugars are not altered in LDKO livers ($n = 5$ mice per group, Student t test).

regulate *Mgat5* transcription, whereas SHP may indirectly regulate transcription of *St3gal6* and *St6gal1*.

Ablation of hepatic Fxr and Shp results in higher hyperbranching and glycan core fucosylation

To assess the functionality of the induction of N-glycosylation genes, we performed glycan profiling on control and LDKO liver lysates (fig. S6A). We found about twofold increase in core fucosylation (Fig. 3A) and hyperbranching (tertiary glycans) in LDKO livers compared to the controls (Fig. 3B), whereas both sialylation and mannosylation were unaltered (fig. S6B). To identify the proteins that were being targeted for altered *N*-glycan processing, we performed glycoproteomics on control and LDKO liver lysates. Figure S6C illustrates an example of the mass spectrum of a glycoform of a liver protein. Gene Ontology analysis of the transcripts encoding for these altered glycoproteins revealed a metabolic or secretory

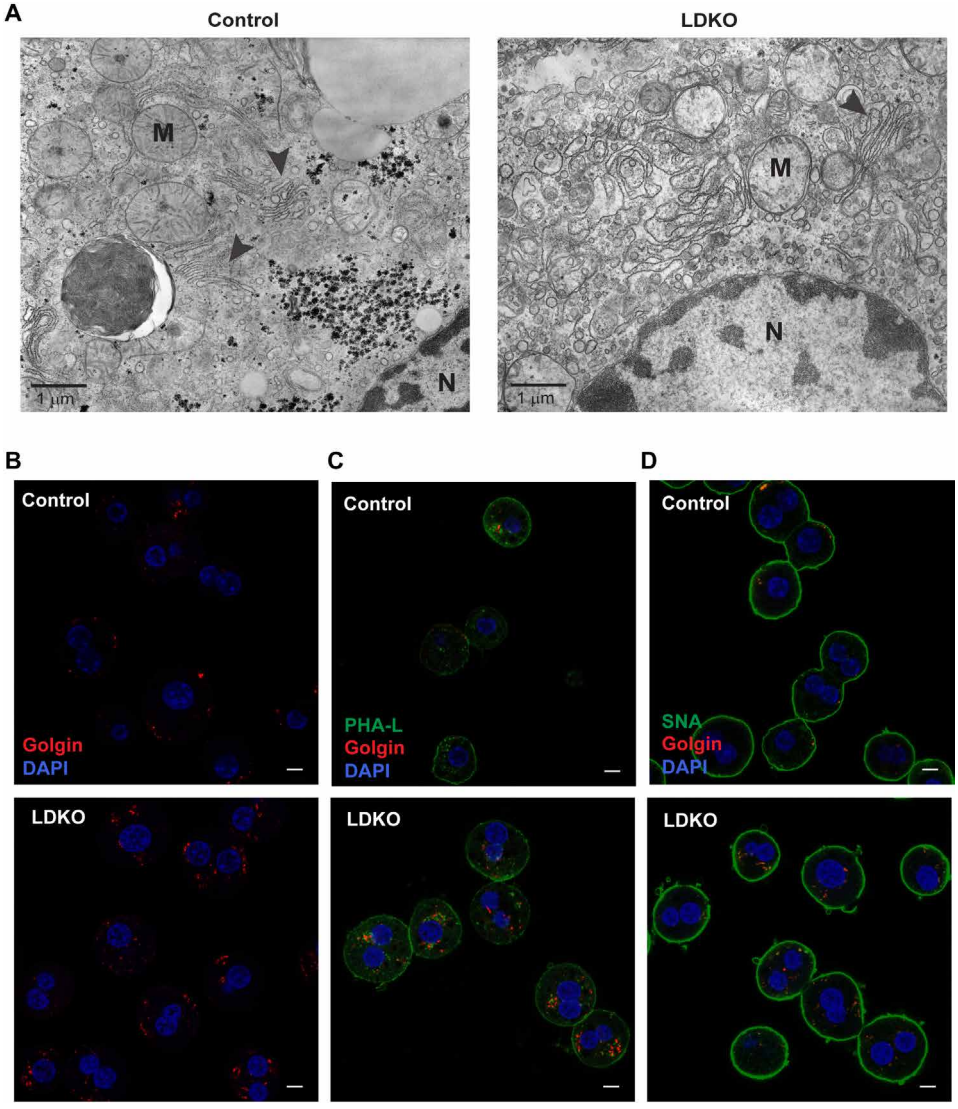

Fig. 5. LDKO hepatocytes exhibit Golgi structural defects. (**A**) Electron microscopy imaging shows unstacked Golgi apparatus (arrowheads) in LDKO livers compared to controls. Scale bar, 1 μm. (**B**) Immunofluorescence staining for a Golgi resident protein, Golgin reveals increased expression in LDKO hepatocytes. DAPI, 4′,6-diamidino-2-phenylindole. This Golgin labeling colocalizes with lectins binding to (**C**) complex and (**D**) sialylated glycans in LDKO proteome (hepatocytes cultured from $n = 3$ mice per group). Scale bars, 10 μm.

function and localization to the extracellular exosome, ER, and lysosome (Fig. 3C). These proteins including, but not limited to, cathepsin Z, lysosomal membrane protein, endoplasmin, haptoglobin, and epoxide hydrolase exhibited increases in more complex glycoforms in LDKO livers (Fig. 3D and fig. S6D). For example, we found that HexNAc(5)Hex(5)Fuc(1)NeuAc(1) glycoform of lysosomal membrane protein is completely absent and replaced by a more complex HexNAc(5)Hex(7)Fuc(1)NeuAc(2) glycoform in LDKO livers. These data are in line with gene expression changes, and consistently, we find complex *N*-glycan decorations in LDKO.

Metabolic and functional consequence of increased glycosylation in LDKO mice

To determine the consequence of elevated glycosylation in LDKO livers, we examined the different cellular fates of glucose, such as glycolysis, pentose phosphate pathway, glycosylation, glycogenesis, and gluconeogenesis (Fig. 4A) (*29*, *30*). In agreement with increased glycosylation, LDKO mice exhibited lower circulating glucose levels (Fig. 4B). Furthermore, the genes regulating glycolysis, pentose phosphate pathway, and gluconeogenesis remained unaltered in LDKO livers (Fig. 4, C to E). However, the low glucose correlated with the severe loss of glycogen stores in LDKO livers as evident by periodic acid–Schiff (PAS) staining (Fig. 4F). Next, we analyzed the intermediates of the hexosamine biosynthesis pathway such as uridine 5′-diphosphate (UDP)–GlcNAc and UDP-GalNAc (*31*–*33*) in LDKO livers, and their levels were comparable despite the increase in demand for N-glycosylation (Fig. 4G). While the hexose intermediates are not limiting, the liver glycogen levels are diminished, circulating glucose is reduced, and N-glycosylation is increased, when the FXR-SHP axis is ablated in the liver.

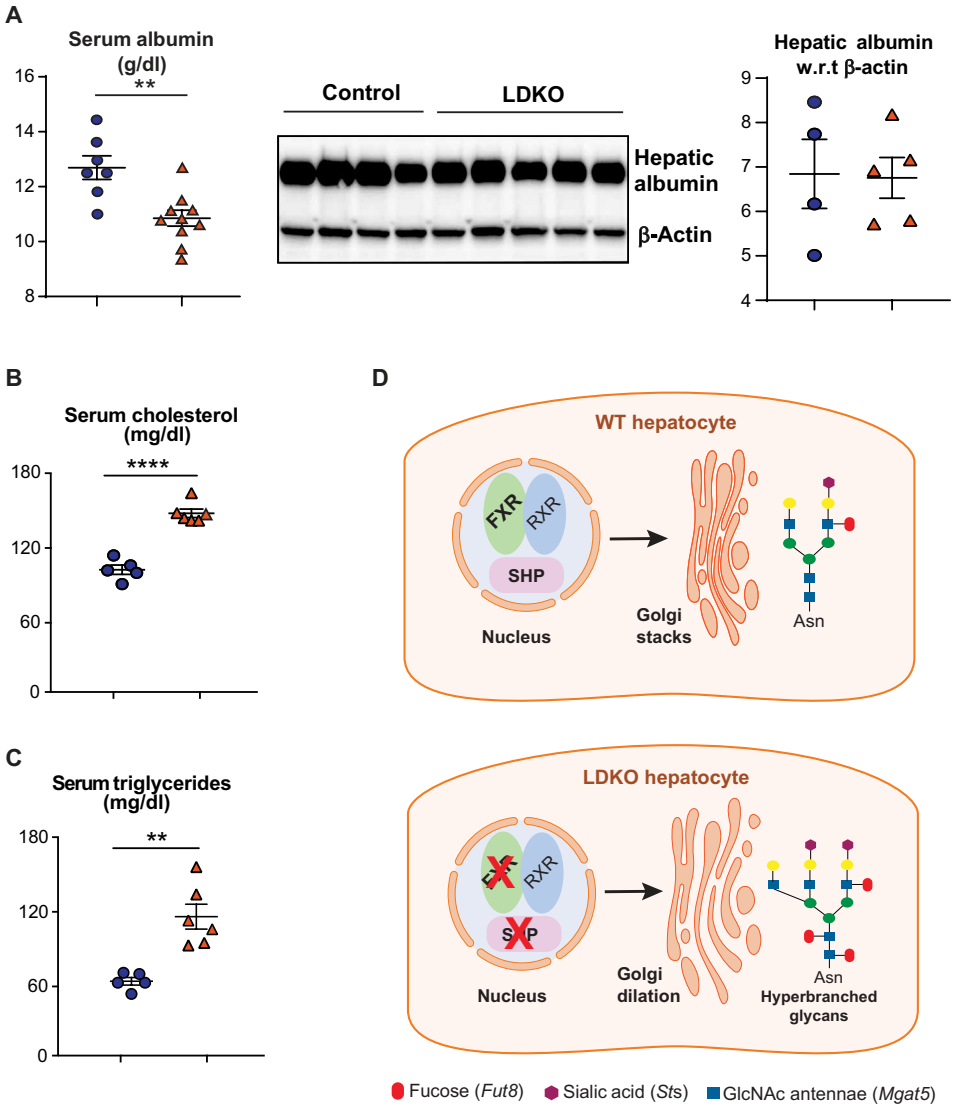

Fig. 6. Hepatic secretory ability is altered upon the loss of FXR and SHP. (**A**) Circulating levels of albumin are reduced in LDKO mice, with no significant change in hepatic albumin levels ($n = 4$ to 9 mice per group, Student t test, $^{**}P < 0.01$). Whereas serum levels of (**B**) cholesterol and (**C**) triglycerides are higher in LDKO mice ($n = 5$ to 9 mice per group; Student t test, $^{**}P < 0.01$ and $^{****}P < 0.0001$). (**D**) Schematic figure displaying unstacked Golgi and hyperbranched N-glycans in an LDKO hepatocyte.

LDKO livers exhibit structural and functional defects in the Golgi apparatus

As *N*-glycan processing occurs in both the ER and the Golgi apparatus (*3*, *5*, *8*), we examined and found that the N-linked glucosyl transferases up-regulated in the LDKOs were specifically associated with the Golgi and not the ER (*34*) except for *Alg10b*, which catalyzes the final step in the synthesis of *N*-glycan moiety (fig. S7A). As unfolded protein response can regulate *N*-glycome (*35*–*38*), we quantified ER stress in LDKO livers by XBP-1 (X-box binding protein 1) splicing assays (*39*–*41*) and gene expression profiling (*42*). We found no changes in them compared to control (fig. S7, B and C). These data confirm that the N-glycosylation and the stress pathways in ER are not affected, but several N-glycosylation genes in the Golgi apparatus are induced in LDKO livers (Fig. 2, A and B). So, using electron microscopy, we examined the Golgi structure and observed unstacked and dilated Golgi in LDKO livers, unlike well-stacked Golgi ribbons in controls (Fig. 5A).

To validate that the loss of FXR-SHP–induced hepatic Golgi expansion and accumulation of N-glycoproteins, we isolated primary hepatocytes from control and LDKO mice and stained them for the resident Golgi-protein, Golgin. LDKO hepatocytes displayed higher Golgin expression than controls (Fig. 5B). In addition, Phaseolus Vulgaris Leucoagglutinin (PHA-L) and Sambucus nigra agglutinin (SNA) were used to stain-branched (complex) glycans and sialic acid moieties, respectively. Both PHA-L and SNA stained the plasma membrane and some of the Golgi as expected (*7*). The amount of PHA-L and SNA staining and its colocalization with Golgin were enhanced in LDKO hepatocytes compared to controls (Fig. 5, C and D). Last, we measured plasma profiles of the secreted products trafficked through the Golgi (*43*, *44*) from LDKO livers. We found that, in the LDKO mice, while hepatic albumin levels were unaffected, serum albumin levels were significantly reduced (Fig. 6A). In addition, the circulating levels of cholesterol and triglycerides were significantly altered in LDKO plasma, compared to controls (Fig. 6, B and C). Together, these

findings reveal that loss of hepatic FXR-SHP axis results in up-regulation of N-glycosylation transcripts, increases in complex glycoforms, defective Golgi structure, and altered secretion in hepatocytes (Fig. 6D), which likely also affects lipoprotein clearance indirectly.

DISCUSSION

Unlike global *Fxr-Shp* double-knockout mice (*12*), the LDKOs did not accumulate excessive bile acids under basal conditions. However, they were defective in their response to a bile acid overload (CA-enriched diet), indicating that the hepatic FXR-SHP axis is necessary for this function.

We serendipitously found a role for FXR and SHP in regulating the N-glycosylation status of liver proteins through RNA-seq data of control and LDKO livers. Only the N-glycosylation specific to Golgi was induced, with no difference in the levels of intracellular *O*-GlcNAcylation or ER N-glycosylation. Particularly, the "branching" glycosyltransferase *Mgat5*, core fucosyltransferase *Fut8*, and sialyltransferases *St3gal6* and *St6gal1* (*7*, *23*, *45*) were induced in the absence of hepatic FXR-SHP axis. We validated the gene expression data and found increases in core fucosylation and triantennary complex branching of glycan moieties on LDKO N-glycoproteins by glycomics.

Challenging hepatocytes with high bile acid concentrations in vitro and 17OHP in vivo both resulted in suppression of genes involved in N-glycosylation. This BA-mediated decrease in glcosylation was also observed in previously published studies (*46*–*48*). Thus, it is unlikely that the increase in BA or 17OHP directly caused the observed up-regulation of glycosyltransferases in LDKO livers.

Next, we tested whether FXR and SHP can individually alter the expression profiles of these glycosyltransferases. Loss of hepatic SHP induced expression of sialyltransferases, whereas FXR activation suppressed *Mgat5* gene, which is responsible for glycan branching, indicating that FXR and SHP coordinate the N-linked glycan landscape at the transcript level in the liver.

To further probe how LDKO mice fuel the increased N-glycosylation in the liver, we examined various glucose metabolic pathways and found no alterations in glycolysis, pentose phosphate pathway, and gluconeogenesis. However, we observed reduced serum glucose levels and hepatic glycogen pools in LDKO mice that could be used through the hexosamine biosynthetic pathways to increase N-glycosylation. Despite increase N-glycans in the LDKO mice, we found no differences in the levels of UDP-GlcNAc and UDP-GalNac in the livers, indicating similar flux through the hexosamine biosynthetic pathway between the LDKO and WT livers and that the hexosamine pathway is not rate limiting in this process.

Since the altered glycosyltransferases in the LDKO mice—*Mgat5, Fut8*, and *St3gals*—are localized only in medial- and trans-Golgi apparatus (*23*, *49*), this indicates a spatial specificity of the hepatic FXR-SHP regulation. To this effect, we did not observe any ER stress in the LDKO livers. The structural defect was localized to the Golgi apparatus in LDKO livers. Furthermore, many of the N-linked glycoproteins present in the exosomes, lysosomes, and ER were up-regulated in the LDKO livers. Not only more complex glycoforms are expressed in LDKO livers but also glycoforms that were not detected in controls. These "hyperglycoforms" in LDKO may alter the function of the protein, resulting in defective signaling pathways.

Last, we observed an altered secretome of LDKO livers, which is consistent with a recent study that predicted that FXR may control hepatocyte secretome (*50*). Our findings provide a mechanism and additional evidence of how the secretory ability of the liver may be altered when the hepatic FXR and SHP axis is deleted. Overall, this study defines a previously unidentified role for FXR and SHP in regulating glycosylation, a less understood posttranslational modification, which is distinct from their conventional role in nutrient homeostasis. Understanding how hepatic FXR-SHP axis specifically regulates Golgi dynamics and N-glycosylation will open new avenues to target various cellular pathways.

MATERIALS AND METHODS

Animals and experimental design

Fxr-floxed and *Shp*-floxed mice, obtained from K. Schoonjans laboratory, were intercrossed to obtain double-floxed homozygous *Fxr-Shp* mice ($Fxr^{fl/fl}$ $Shp^{fl/fl}$). Furthermore, these $Fxr^{fl/fl}$ $Shp^{fl/fl}$ (control) mice were bred with mice expressing the Cre-recombinase under the control of albumin promoter (AlbCre mice, Envigo/Harlan laboratories) to obtain liver-specific double knockouts ($Fxr^{fl/fl}$ $Shp^{fl/fl}$ $AlbCre^{+}$, LDKO). The mice were maintained on a C57BL/6J background and housed on a standard 12-hour light/12-hour dark cycle. Both the control and LDKO mice were born in regular Mendelian ratios. To study how LDKO mice respond to BA-induced stress, we fed LDKO and control mice with normal chow or 1% CA diet for 5 days. Plasma, liver, gall bladder, and ileum were collected between Zeitgeber times ZT4 to ZT6 (n = 6 to 12 mice per group). Fasted C57BL/6J mice (Envigo/Harlan laboratories) were gavaged with either vehicle [1% methylcellulose and 1% TritonX-100 in phosphate-buffered saline (PBS)] or FXR agonist GW4064 (50 mg/kg). Mice were gavaged twice, first in the evening and second in the morning, and euthanized 3 hours after second gavage (n = 5 mice per group). To examine the role for 17OHP, we injected WT mice with 17OHP (125 mg/kg, i.p) or corn oil twice on the first day, followed by once daily injections for four additional days. All the experiments were carried out on 10- to 12-week-old male mice, fasted for 8 to 10 hours unless specified as outlined in the *Guide for the Care and Use of Laboratory Animals*, the National Academy of Sciences (NIH publication 86-23, revised 1985), and approved by the Institutional Animal Care and Use Committee at University of Illinois at Urbana-Champaign.

Genotyping

Mouse tails were clipped during weaning to obtain genomic DNA. Tails were lysed using DirectPCR tail lysis buffer (Viagen Biotech) and proteinase K by an overnight incubation at 55°C. Proteinase K was heat-inactivated for 1 to 2 hours, and PCR was performed on the DNA isolated using primers listed in table S1.

Chemicals

Methylcellulose was obtained from Sigma-Aldrich (catalog no. 0262), GW4064 was obtained from Cayman Chemicals and 17OHP (Sigma-Aldrich).

Primary hepatocytes isolated from C57BL/6J mice were incubated with 100 μM DCA (Sigma-Aldrich) for 6 hours (n = 2 mice per group, three technical replicates).

Serum biochemistry

Blood was collected and centrifuged at 7000 to 8000*g* for 10 min. The plasma samples collected were tested for ALT and AST enzymes using Infinity ALT/GPT (glutamic-pyruvic transaminase) and AST/GOT (glutamic-oxaloacetic transaminase) kits (Thermo Fisher Scientific).

Plasma BA levels were measured using a colorimetric BA assay kit (Genway) according to the manufacturer's protocol. The circulating albumin levels were quantitated using the Albumin [BCG (Bromocresol Green)] Colorimetric Assay Kit (Biovision). Control and LDKO mice (n = 5 to 6 mice per group) were fasted for four hours before collecting blood. Fresh plasma was analyzed for lipid metabolites by fast-protein liquid chromatography at Perelman School of Medicine, University of Pennsylvania. For fasting blood glucose measurements, control and LDKO mice were fasted for 12 hours, and blood glucose was measured by tail bleeds using one-touch glucometer. Serum 17OHP levels were measured by mass spectroscopy at Roy J Carver Biotechnology Center Metabolomics Facility at University of Illinois, Urbana-Champaign.

Tissue BA assay

For hepatic and intestinal BA analysis, about 100 mg of liver tissue or whole ileum was homogenized in 75% ethanol, followed by a 2-hour incubation at 50°C and centrifugation at 15,000*g* for 10 min. The supernatant was diluted with 1× PBS and used to measure BA content in the liver or intestine, respectively, using the colorimetric BA Assay Kit (GenWay) according to the manufacturer's protocol. The BA levels were normalized to the weight of the tissue used. For biliary BA measurements, intact gall bladders from mice were punctured to obtain the content, which was further diluted with 1× PBS and analyzed for BA pools.

Histology

Liver tissues from all the mouse cohorts were fixed in 10% neutral-buffered formalin overnight, subsequently dehydrated in increasing concentrations of ethanol (70 to 100%) and xylene, and lastly embedded in paraffin. Liver sections (5 μm thick) were cut, deparaffinized, and stained with hematoxylin and eosin using standard histological protocols. These sections were also stained with periodic acid and Schiff's reagent for PAS staining. Briefly, the deparaffinized sections were stained with 0.5% periodic acid for 10 min, followed by wash in water and incubation in Schiff's solution for 30 min. Next, slides are rinsed in 0.55% potassium metabisulfite for 30 s and washed in running warm tap water for 10 min to develop the pink color. Last, the sections were counterstained with hematoxylin, mounted, and imaged.

RNA-seq analysis

RNA was isolated from control and LDKO livers (n = 3 per group) using the RNeasy Tissue Mini Kit (Qiagen). RNA quality was tested using an Agilent bioanalyzer by the Functional Genomics Core at the Roy J. Carver Biotechnology Center, UIUC (University of Illinois, Urbana-Champaign). HiSeq libraries were prepared, and 100–base pair (bp) paired-end Illumina sequencing was performed on a HiSeq 4000 at the high-throughput sequencing and genotyping unit, UIUC. Reads were processed for quality using Trimmomatic (*51*) and aligned to the mouse genome (mm10) using STAR (*52*). Gene expression was determined as fragments per kilobase million using count and differential expression values obtained from DESeq2 (*53*) and HTseq (*54*). Fold change of >1.5 and <0.67 was considered significant. Gene Ontology pathway and cellular component analysis were performed using DAVID (Database for Annotation, Visualization, and Integrated Discovery) and mapped using Enrichment maps plugin in Cytoscape. Mouse reference gene set served as background. The RNA-seq data discussed in this publication have been deposited in NCBI's Gene Expression Omnibus (GEO) (*55*) and are accessible through GEO Series accession number GSE164447 (www.ncbi.nlm.nih.gov/geo/query/acc.cgi?acc=GSE164447).

Identifying DNA binding motifs

The gene sequences were retrieved from the Ensembl genome browser, release 102 (*56*). These sequences were then run using FIMO (Find Individual Motif Occurrences) software (*57*). FIMO uses a position-dependent scoring matrix that describes the score of each possible nucleotide at each position in the given sequence. Motifs containing or resembling the canonical "IR1 (*AGGTCAnTGACCT*) and ER2 (*TGACCTnnAGGTCA*) motifs" were identified and compared with the binding peaks identified using the ChIP-seq dataset (*27*, *28*).

Quantitative real-time PCR and splicing assay analysis

RNA was isolated from snap-frozen livers (n = 4 to 5 per group) using TRIzol (Invitrogen) and reverse-transcribed for gene expression analysis by SYBR Green–based Real-Time Quantitative Reverse Transcription PCR (qRT-PCR) using mouse-specific primer sets listed in table S2. Relative gene expression was calculated by delta-delta *C*t method and was normalized to *36B4* as loading control. For Xbp-1 splicing assay, the complementary DNA samples from both control and LDKO livers were run on a 5% nondenaturing polyacrylamide gel electrophoresis (PAGE) gel to examine its spliced isoforms. Percentage (%) exclusion for the variably spliced region was calculated with ImageLab software (Bio-Rad) as [(exon inclusion band intensity)/(exon inclusion band intensity + exon exclusion band intensity) × 100].

Detection of *O*-GlcNAc by Western blot

Liver tissues were homogenized in Tissue Protein Extraction Reagent (Thermo Fisher Scientific) using the gentleMACS dissociator (Miltenyi Biotec). Protein (30 μm) was run out on a PAGE gel and transferred to a nitrocellulose membrane. Membranes were incubated overnight with antibodies to *O*-GlcNAc (RL2, Thermo Fisher Scientific) and glyceraldehyde-3-phosphate dehydrogenase (Abcam). Visualization was done using the Li-Cor Odyssey and analysis using the Li-Cor Image Studio Software.

Extraction of proteins from mouse liver for glycomics, glycoproteomics, and proteomics

Control and LDKO liver tissues (n = 5 mice per group) were tested for glycan structural diversity in glycoproteins using matrix-assisted laser desorption/ionization–time-of-flight (*45*) and mass spectrometry (MALDI-TOF-MS) at Complex Carbohydrate Research Center, University of Georgia. Briefly, about 100 mg of liver tissue was homogenized in a 1:1 ratio of ice-cold methanol/water. Chloroform:methanol:water at the ratio of 4:8:3 was added, mixed vigorously, and left to incubate at room temperature for approximately 2 hours on a bench rocker. The sample was then centrifuged at 4°C, 3000 rpm for 15 min to separate the precipitated tissue proteins from the supernatant glycolipids layer. The chloroform:methanol:water extraction was repeated two more times. The protein pellet was blown for a few minutes under a stream of nitrogen, and 1 ml of ice-cold water, along with 4 ml of ice-cold acetone, was added for acetone precipitation at −20°C. After about 4 hours, the sample was centrifuged at 4°C, 3000 rpm for 15 min, and the supernatant was discarded. Acetone precipitation was repeated one more time, and lastly, the pellets were processed using only 4 ml of ice-cold acetone, following the same procedure. The pellets were then dried under the nitrogen stream and stored at −80°C for further analysis.

Glycomics analysis

About 5 mg of protein pellet was resuspended in 50 mM ammonium bicarbonate buffer and digested with trypsin for 24 hours at 37°C, followed by purification by passing through a C18 solid-phase cartridge after inactivating trypsin by heating at 95°C for 5 min. The eluted peptides were treated twice with peptide *N*-glycosidase F (PNGaseF) for a total incubation time of 18 hours. The released N-glycans were separated from the peptides by passing through a C18 solid-phase cartridge and were dried by lyophilization. These N-glycans were permethylated with methyl iodide for 10 min at room temperature with shaking. The reaction was quenched by adding water, and the permethylated glycans were extracted in dichloromethane, dried under a stream of nitrogen, and analyzed by MALDI-TOF-MS by using DHB (2,5-dihydroxybenzoic acid) as the matrix (*58*).

For 17OHP experiments, about 50 mg of liver tissue was washed with PBS two times and homogenized in 50 mM ammonium bicarbonate buffer using a 20-gauge needle and syringe. The sample was probe-sonicated for 2 min, followed by ultrafiltration thrice using 10-kDa centrifuge filters (MilliporeSigma Amicon, UFC501024). The protein solution from the filter was collected in the ammonium bicarbonate buffer with PNGaseF and incubated at 37°C for 48 hours. The N-glycans were then purified, permethylated, and analyzed by MALDI-MS as mentioned above.

Glycoproteomics analysis

About 1 mg of proteins extracted was dissolved in 50 mM ammonium bicarbonate buffer. Dithiothreitol solution (17 mg/ml) was added to the samples and incubated at 37°C for 90 min, followed by incubation with iodoacetamide solution (65 mg/ml) at room temperature for 90 min in the dark for carbamidomethylation. The sample was dialyzed against double-distilled water and digested by trypsin (0.4 μg/μl; Promega) at a trypsin to protein ratio of 1:40 and incubated at 37°C for 12 hours. The digestion was terminated by heating at 95°C for 5 min, desalted by C18 solid-phase extraction cartridges, and then samples were dried under speed vacuum. The peptides and glycopeptides were subsequently redissolved in 0.1% formic acid in water. The digests were enriched for the glycopeptides by using the ProteoExtract Glycopeptide Enrichment Kit (Millipore, MA) and stored at −80°C until analysis by nano–liquid chromatography–tandem MS (LC-MS/MS).

Desalted liver protein digests were analyzed on an Orbitrap Fusion Tribrid mass spectrometer (Thermo Fisher Scientific, MA) equipped with a nanospray ion source and connected to a Dionex binary solvent system. Prepacked nano-LC columns of 15 cm length with 75 μm internal diameter, filled with 3-μm C18 material, were used for chromatographic separation of digests. Precursor ion scan was performed at 120,000 resolution in an Orbitrap analyzer, and precursors at a time frame of 3 s were selected for subsequent fragmentation using higher-energy collisional dissociation (HCD) at a normalized collision energy of 28 and collision-induced dissociation (CID) at a normalized collision energy of 40. The threshold for triggering an MS/MS event was set to 500 counts. The fragment ions were analyzed on Orbitrap after HCD and CID fragmentation at a resolution of 30,000. Charge-state screening was enabled, and precursors with unknown charge state or a charge state of +1 were excluded (positive ion mode). Dynamic exclusion was enabled with an exclusion duration of 30 s.

The LC-MS/MS spectra of the tryptic digest of proteins were searched against mouse protein database in.fasta format (downloaded from uniport) using Byonic 2.3 software with trypsin as the digestion enzyme. Carbamidomethylation of cysteine and oxidation of methionine were selected as variable modifications. Common mammalian N-glycans were used as variable modifications on asparagines. The LC-MS/MS spectra were analyzed manually for the glycopeptide fragmentation on HCD and CID with the support of Xcalibur 3.0.63 software. The spectra of glycopeptides were evaluated for the glycan neutral loss pattern, oxonium ions, and the glycopeptide fragmentations and identified the glycans. For the relative ratio calculation, the peak area of the glycoforms was extracted manually using the Xcalibur 3.0.63 software. Unannotated glycopeptides were identified on the basis of the presence of oxonium ions and neutral losses on the spectra of glycopeptides.

Nucleotide sugar extraction and detection

Sugars from liver tissues were extracted as described previously (*59*). Approximately 50 mg of mouse liver tissue was homogenized in 1 ml of cold 80% ethanol in a gentleMACS (Miltenyi Biotec) dissociator. Tissue lysates were centrifuged at 8000*g* for 20 min at 4°C, and the supernatant was evaporated in a vacuum centrifuge overnight. The evaporated samples were dissolved in 9% butanol, and lipids were removed by three extractions with 90% butanol. The lower aqueous fraction was evaporated overnight by vacuum centrifuge. Samples were resuspended in 5 mM ammonium bicarbonate, and sugar nucleotides were extracted using EnviCarb graphitized carbon columns (Supelco). Columns were prepared by washing with 3 ml of 80% acetonitrile and 0.1% trifluoroacetic acid, followed by 2 ml of water. Samples were loaded, and the column was washed with 2 ml of water and 2 ml of 25% acetonitrile, followed by 2 ml of 50 mM TEAA (Triethylammonium acetate) buffer. Samples were eluted with 2 ml of 25% acetonitrile and 50 mM TEAA. Eluate was evaporated overnight in a vacuum centrifuge and dissolved in 240 μl of 40 mM sodium phosphate buffer.

A Dionex (Thermo Fisher Scientific) HPIC (High Pressure Ion Chromatography) system consisting of a Dionex ICS-6000, CarboPac PA1 column 2x250, and PA1 guard column 2x50 under the control of Chromeleon 7 software was used for analysis. The program involved a gradient made of the following solutions: A = dionized water; B = 1 mM NaOH; C = 1 mM NaOH/1 M NaOAC. The gradient was isocratic B followed by a 20-min gradient up to 60% C. A step up to 100 B was used to clean the column before an equilibration back to 100 A. Ultraviolet absorbances were collected at 260 nm. Concentrations of nucleotide sugars detected were normalized to wet weight of tissues.

Lectin staining

Liver sections (5 μm thick) from control and LDKO mice were cut, deparaffinized, and stained for lectins such as UEA (Ulex Europaeus Agglutinin) (binds fucose), PHA-L (binds complex glycans), and SNA (binds sialic acid) from Vector Laboratories. Briefly, sections were blocked with Carbo-free Blocking solution (SP-5040, Vector Laboratories) for 30 min at room temperature, followed by fluorescently labeled lectin in PBS for 30 min at room temperature. The slides were then washed twice in PBST (Phosphate Buffered Saline with Triton X-100) and stained, mounted with Vectashield Hardset mounting media (H-1400, Vector Laboratories), and imaged using confocal microscope LSM 710 at Institute for Genomic Biology Core facility, UIUC using 488-nm laser, and a red psuedocolor was assigned to it.

Immunostaining of primary hepatocytes

Primary hepatocytes from control and LDKO mice were isolated using a two-step collagenase perfusion technique using 3000 U collagenase type I from Worthington. Cells were layered onto a 30% Percoll gradient and centrifuged at 600 rpm for 10 min. The pellet, rich in live hepatocytes, was then washed, cultured in growing medium (Williams E media supplemented with 1× insulin-transferrin-selenium solution from Gibco, 1× penicillin/streptomycin, and 1× L-glutamine), and plated in collagen-coated fluorodishes. Media was changed 2 hours after plating to remove dead, nonadherent cells, and the cells were fixed in 4% paraformaldehyde for 10 to 15 min after two more hours, followed by lectin staining as mentioned above. These cells are further permeabilized with 1× PBS with 0.2% Triton X-100 and 1% normal goat serum for 10 min at room temperature and then incubated in the blocking buffer (1× PBS + 1% normal goat serum) for 30 min. The primary antibody for Golgin 97 (catalog no. 13192, Cell Signaling Technology) was applied to the sections at 1:100 concentration and incubated overnight at 4°C. Next, the sections were washed in the blocking buffer, and secondary fluorescent antibodies (anti-rabbit Alexa Fluor 594) were applied for 1 hour at room temperature. Last, the cells were incubated with NucBlue nuclear staining probes (R37606, Thermo Fisher Scientific) for 15 min at room temperature and then imaged on a Zeiss LSM 710 microscope at Institute for Genomic Biology core facility, UIUC.

Transmission electron microscopy

Liver sections (1 mm thick) were fixed in 2.5% glutaraldehyde (pH 7) for 2 to 3 hours, followed by postfixation with 1% osmium tetroxide (OsO_4) in 0.1 M cacodylate buffer for 60 min. These sections are then dehydrated through ethanol series and embedded using epoxy resin. Ultrathin sections are cut and left to dry, followed by imaging using transmission electron microscopy.

Western blot

Total proteins were isolated from ~50 mg of snap-frozen liver tissue by homogenizing in 600 µl of cold radioimmunoprecipitation assay buffer containing 10 mM tris-Cl (pH 8), 1 mM EDTA, 0.5 mM EGTA, 1% Triton X-100, 0.5% sodium deoxycholate, 140 mM NaCl, 0.1% SDS, and phosphatase and protease inhibitors (one tablet per 10 ml of buffer; catalog nos. 4906837001 and 4693159001). Samples were sonicated in a water bath to shear DNA and clarified by centrifugation. Protein concentration was measured using the DC (detergent compatible) Protein Assay Kit (Bio-Rad, 5000112). Proteins (~20 µg) were resolved on a 4 to 20% TGX (Tris-Glycine eXtended) gel (Bio-Rad) and transferred semidry using "Mixed MW" program on the Bio-Rad Trans Blot Turbo System onto a nitrocellulose membrane with 0.45-µm pore size (Bio-Rad). Membranes were blocked for 1 hour at room temperature using tris-buffered saline containing 5% nonfat dry milk and 0.1% Tween 20 (TBST). Membranes were then incubated with primary antibody against albumin (1:1000; Cell Signaling Technology, no. 4929) overnight at 4°C. The membranes were then washed thrice with TBST, followed by incubation with an anti-rabbit horseradish peroxidase–conjugated secondary antibody (1:5000; Bio-Rad, no. 1706515) for 1 hour. Membranes were then visualized on the ChemiDoc MP using the Clarity Western ECL Kit (Bio-Rad).

Statistical analysis

One-way analysis of variance (ANOVA) with post hoc Bonferroni test was used for comparison of multiple groups or unpaired Student's *t* test for comparison between two groups. $P < 0.05$ was considered significant.

SUPPLEMENTARY MATERIALS

Supplementary material for this article is available at http://advances.sciencemag.org/cgi/content/full/7/17/eabf4865/DC1

View/request a protocol for this paper from *Bio-protocol*.

REFERENCES AND NOTES

1. M. E. Taylor, K. Drickamer, *Introduction to Glycobiology* (Oxford Univ. Press, ed. 2, 2006), p. 1733.
2. G. W. Hart, C. M. West, Nucleocytoplasmic Glycosylation, in Essentials of Glycobiology, A. Varki, R. D. Cummings, J. D. Esko, H. H. Freeze, P. Stanley, C. R. Bertozzi, G. W. Hart, M. E. Etzler, Eds. (Cold Spring Harbor Laboratory Press, Cold Spring Harbor, New York, ed. 2, 2009), Chapter 17. Available from: https://www.ncbi.nlm.nih.gov/books/NBK1915/?report=classic.
3. H. Schachter, Complex N-glycans: The story of the yellow brick road. *Glycoconj. J.* **31**, 1–5 (2014).
4. N. Cherepanova, S. Shrimal, R. Gilmore, N-linked glycosylation and homeostasis of the endoplasmic reticulum. *Curr. Opin. Cell Biol.* **41**, 57–65 (2016).
5. F. Schwarz, M. Aebi, Mechanisms and principles of N-linked protein glycosylation. *Curr. Opin. Struct. Biol.* **21**, 576–582 (2011).
6. M. Aebi, N-linked protein glycosylation in the ER. *Biochim. Biophys. Acta Mol. Cell Res.* **1833**, 2430–2437 (2013).
7. P. Stanley, Golgi glycosylation. *Cold Spring Harb. Perspect. Biol.* **3**, a005199 (2011).
8. H. Lodish, A. Berk, S. L. Zipursky, P. Matsudaira, D. Baltimore, J. Darnell, Molecular Cell Biology (W. H. Freeman, New York, ed. 4, 2000), Section 17.7, Protein Glycosylation in the ER and Golgi Complex. Available from: https://www.ncbi.nlm.nih.gov/books/NBK21744/.
9. N. Tanichi, H. Korekane, Branched N-glycans and their implications for cell adhesion, signaling and clinical applications for cancer biomarkers and in therapeutics. *BMB Rep.* **44**, 772–781 (2011).
10. A. Feizi, F. Gatto, M. Uhlen, J. Nielsen, Human protein secretory pathway genes are expressed in a tissue-specific pattern to match processing demands of the secretome. *npj Syst. Biol. Appl.* **3**, 22 (2017).
11. J. Zhu, Z. Sun, K. Cheng, R. Chen, M. Ye, B. Xu, D. Sun, L. Wang, J. Liu, F. Wang, H. Zou, Comprehensive mapping of protein N-glycosylation in human liver by combining hydrophilic interaction chromatography and hydrazide chemistry. *J. Proteome Res.* **13**, 1713–1721 (2014).
12. S. Anakk, M. Watanabe, S. A. Ochsner, N. J. McKenna, M. J. Finegold, D. D. Moore, Combined deletion of *Fxr* and *Shp* in mice induces Cyp17a1 and results in juvenile onset cholestasis. *J. Clin. Invest.* **121**, 86–95 (2011).
13. S. Anakk, M. Bhosale, V. A. Schmidt, R. L. Johnson, M. J. Finegold, D. D. Moore, Bile acids activate YAP to promote liver carcinogenesis. *Cell Rep.* **5**, 1060–1069 (2013).
14. B. Goodwin, S. A. Jones, R. R. Price, M. A. Watson, D. D. McKee, L. B. Moore, C. Galardi, J. G. Wilson, M. C. Lewis, M. E. Roth, P. R. Maloney, T. M. Willson, S. A. Kliewer, A regulatory cascade of the nuclear receptors FXR, SHP-1, and LRH-1 represses bile acid biosynthesis. *Mol. Cell* **6**, 517–526 (2000).
15. J. Y. L. Chiang, Bile acids: Regulation of synthesis. *J. Lipid Res.* **50**, 1955–1966 (2009).
16. P. A. Dawson, in *Physiology of the Gastrointestinal Tract* (2012), vol. 2, pp. 1461–1484.
17. D. W. Russell, Fifty years of advances in bile acid synthesis and metabolism. *J. Lipid Res.* **50**, S120–S125 (2009).
18. A. Perino, K. Schoonjans, Another Shp on the horizon for bile acids. *Cell Metab.* **20**, 203–205 (2014).
19. M. Makishima, A. Y. Okamoto, J. J. Repa, H. Tu, R. M. Learned, A. Luk, M. V. Hull, K. D. Lustig, D. J. Mangelsdorf, B. Shan, Identification of a nuclear receptor for bile acids. *Science* **284**, 1362–1365 (1999).
20. M. O. Hoeke, J. Heegsma, M. Hoekstra, H. Moshage, K. N. Faber, Human FXR regulates SHP expression through direct binding to an LRH-1 binding site, independent of an IR-1 and LRH-1. *PLOS ONE* **9**, e88011 (2014).
21. G. W. Hart, Y. Akimoto, The O-GlcNAc modification, in *Essentials of Glycobiology*, A. Varki, R. D. Cummings, J. D. Esko, H. H. Freeze, P. Stanley, C. R. Bertozzi, G. W. Hart, M. E. Etzler, Eds. (Cold Spring Harbor Laboratory Press, ed. 2, 1999), pp. 183–193.
22. I. Brockhausen, H. Schachter, P. Stanley, O-GalNAc Glycans, in Essentials of Glycobiology, A. Varki, R. D. Cummings, J. D. Esko, H. H. Freeze, P. Stanley, C. R. Bertozzi, G. W. Hart, M. E. Etzler, Eds. (Cold Spring Harbor Laboratory Press, Cold Spring Harbor, New York, ed 2, 2009). Chapter 9. PMID: 20301232.
23. X. Zhang, Y. Wang, Glycosylation quality control by the golgi structure. *J. Mol. Biol.* **428**, 3183–3193 (2016).
24. X. Li, X. Wang, Z. Tan, S. Chen, F. Guan, Role of glycans in cancer cells undergoing epithelial–mesenchymal transition. *Front. Oncol.* **6**, 33 (2016).
25. N. Taniguchi, Y. Kizuka, Glycans and cancer: Role of N-glycans in cancer biomarker, progression and metastasis, and therapeutics. *Adv. Cancer Res.* **126**, 11–51 (2015).
26. B. Blomme, C. Van Steenkiste, N. Callewaert, H. Van Vlierberghe, Alteration of protein glycosylation in liver diseases. *J. Hepatol.* **50**, 592–603 (2009).

27. A. M. Thomas, S. N. Hart, B. Kong, J. Fang, X. B. Zhong, G. L. Guo, Genome-wide tissue-specific farnesoid X receptor binding in mouse liver and intestine. *Hepatology* **51**, 1410–1419 (2010).
28. Y. C. Kim, S. Byun, Y. Zhang, S. Seok, B. Kemper, J. Ma, J. K. Kemper, Liver ChIP-seq analysis in FGF19-treated mice reveals SHP as a global transcriptional partner of SREBP-2. *Genome Biol.* **16**, 268 (2015).
29. M. Watford, What is the metabolic fate of dietary glucose? *Trends Biochem. Sci.* **13**, 329–330 (1988).
30. C. Bouché, S. Serdy, C. R. Kahn, A. B. Goldfine, The cellular fate of glucose and its relevance in type 2 diabetes. *Endocr. Rev.* **25**, 807–830 (2004).
31. M. G. Buse, Hexosamines, insulin resistance, and the complications of diabetes: Current status. *Am. J. Physiol. Endocrinol. Metab.* **290**, E1–E8 (2005).
32. A. Vasconcelos-Dos-Santos, I. A. Oliveira, M. C. Lucena, N. R. Mantuano, S. A. Whelan, W. B. Dias, A. R. Todeschini, Biosynthetic machinery involved in aberrant glycosylation: Promising targets for developing of drugs against cancer. *Front. Oncol.* **5**, 138 (2015).
33. S. Marshall, V. Bacote, R. R. Traxinger, Discovery of a metabolic pathway mediating glucose-induced desensitization of the glucose transport system: Role of hexosamine biosynthesis in the induction of insulin resistance. *J. Biol. Chem.* **266**, 4706–4712 (1991).
34. C. Veit, J. König, F. Altmann, R. Strasser, Processing of the terminal alpha-1,2-linked mannose residues from oligomannosidic n-glycans is critical for proper root growth. *Front. Plant Sci.* **9**, 1807 (2018).
35. D. T. W. Ng, E. D. Spear, P. Walter, The unfolded protein response regulates multiple aspects of secretory and membrane protein biogenesis and endoplasmic reticulum quality control. *J. Cell Biol.* **150**, 77–88 (2000).
36. M. Y. Wong, K. Chen, A. Antonopoulos, B. T. Kasper, M. B. Dewal, R. J. Taylor, C. A. Whittaker, P. P. Hein, A. Dell, J. C. Genereux, S. M. Haslam, L. K. Mahal, M. D. Shoulders, XBP1s activation can globally remodel N-glycan structure distribution patterns. *Proc. Natl. Acad. Sci. U.S.A.* **115**, E10089–E10098 (2018).
37. M. B. Dewal, A. S. DiChiara, A. Antonopoulos, R. J. Taylor, C. J. Harmon, S. M. Haslam, A. Dell, M. D. Shoulders, XBP1s links the unfolded protein response to the molecular architecture of mature N-glycans. *Chem. Biol.* **22**, 1301–1312 (2015).
38. K. L. P. Stevens, A. L. Black, K. M. Wells, K. Y. B. Yeo, R. F. L. Steuart, C. J. Stirling, B. L. Schulz, C. J. Mousley, Diminished Ost3-dependent N-glycosylation of the BiP nucleotide exchange factor Sil1 is an adaptive response to reductive ER stress. *Proc. Natl. Acad. Sci. U.S.A.* **114**, 12489–12494 (2017).
39. H. Yoshida, T. Matsui, A. Yamamoto, T. Okada, K. Mori, XBP1 mRNA is induced by ATF6 and spliced by IRE1 in response to ER stress to produce a highly active transcription factor. *Cell* **107**, 881–891 (2001).
40. M. Calfon, H. Zeng, F. Urano, J. H. Till, S. R. Hubbard, H. P. Harding, S. G. Clark, D. Ron, IRE1 couples endoplasmic reticulum load to secretory capacity by processing the XBP-1 mRNA. *Nature* **415**, 92–96 (2002).
41. P. Walter, D. Ron, The unfolded protein response: From stress pathway to homeostatic regulation. *Science* **334**, 1081–1086 (2011).
42. K. Bambino, C. Zhang, C. Austin, C. Amarasiriwardena, M. Arora, J. Chu, K. C. Sadler, Inorganic arsenic causes fatty liver and interacts with ethanol to cause alcoholic liver disease in zebrafish. *Dis. Model. Mech.* **11**, dmm031575 (2018).
43. R. J. Schulze, M. B. Schottm, C. A. Casey, P. L. Tuma, M. A. McNiven, The cell biology of the hepatocyte: A membrane trafficking machine. *J. Cell Biol.* **218**, 2096–2112 (2019).
44. S. Mukherjee, F. R. Maxfield, Cholesterol: Stuck in traffic. *Nat. Cell Biol.* **1**, E37–E38 (1999).
45. Z. Roth, G. Yehezkel, I. Khalaila, Identification and quantification of protein glycosylation. *Int. J. Carbohydr. Chem.* **2012**, 1–10 (2012).
46. R. Sharma, F. Quilty, J. F. Gilmer, A. Long, A.-M. Byrne, Unconjugated secondary bile acids activate the unfolded protein response and induce golgi fragmentation via a src-kinase-dependant mechanism. *Oncotarget* **8**, 967–978 (2017).
47. A. M. Byrne, R. Sharma, G. Duggan, D. Kelleher, A. Long, Deoxycholic acid impairs glycosylation and fucosylation processes in esophageal epithelial cells. *Glycobiology* **22**, 638–648 (2012).
48. A.-M. Byrne, E. Foran, R. Sharma, A. Davies, C. Mahon, J. O'Sullivan, D. O'Donoghue, D. Kelleher, A. Long, Bile acids modulate the Golgi membrane fission process via a protein kinase Cη and protein kinase D-dependent pathway in colonic epithelial cells. *Carcinogenesis* **31**, 737–744 (2010).
49. P. Stanley, H. Schachter, N. Taniguchi, N-Glycans, in Essentials of Glycobiology, A. Varki, R. D. Cummings, J. D. Esko, H. H. Freeze, P. Stanley, C. R. Bertozzi, G. W. Hart, M. E. Etzler, Eds. (Cold Spring Harbor Laboratory Press, Cold Spring Harbor, New York, ed. 2, 2009), Chapter 8. PMID: 20301244.
50. G. A. Preidis, K. H. Kim, D. D. Moore, Nutrient-sensing nuclear receptors PPARα and FXR control liver energy balance. *J. Clin. Invest.* **127**, 1193–1201 (2017).
51. A. M. Bolger, M. Lohse, B. Usadel, Trimmomatic: A flexible trimmer for Illumina sequence data. *Bioinformatics* **30**, 2114–2120 (2014).
52. A. Dobin, C. A. Davis, F. Schlesinger, J. Drenkow, C. Zaleski, S. Jha, P. Batut, M. Chaisson, T. R. Gingeras, STAR: Ultrafast universal RNA-seq aligner. *Bioinformatics* **29**, 15–21 (2013).
53. M. I. Love, W. Huber, S. Anders, Moderated estimation of fold change and dispersion for RNA-seq data with DESeq2. *Genome Biol.* **15**, 550 (2014).
54. S. Anders, P. T. Pyl, W. Huber, HTSeq—A Python framework to work with high-throughput sequencing data. *Bioinformatics* **31**, 166–169 (2015).
55. R. Edgar, M. Domrachev, A. E. Lash, Gene expression omnibus: NCBI gene expression and hybridization array data repository. *Nucleic Acids Res.* **30**, 207–210 (2002).
56. A. D. Yates, P. Achuthan, W. Akanni, J. Allen, J. Allen, J. Alvarez-Jarreta, M. R. Amode, I. M. Armean, A. G. Azov, R. Bennett, J. Bhai, K. Billis, S. Boddu, J. C. Marugán, C. Cummins, C. Davidson, K. Dodiya, R. Fatima, A. Gall, C. G. Giron, L. Gil, T. Grego, L. Haggerty, E. Haskell, T. Hourlier, O. G. Izuogu, S. H. Janacek, T. Juettemann, M. Kay, I. Lavidas, T. Le, D. Lemos, J. G. Martinez, T. Maurel, M. M. Dowall, A. M. Mahon, S. Mohanan, B. Moore, M. Nuhn, D. N. Oheh, A. Parker, A. Parton, M. Patricio, M. P. Sakthivel, A. I. A. Salam, B. M. Schmitt, H. Schuilenburg, D. Sheppard, M. Sycheva, M. Szuba, K. Taylor, A. Thormann, G. Threadgold, A. Vullo, B. Walts, A. Winterbottom, A. Zadissa, M. Chakiachvili, B. Flint, A. Frankish, S. E. Hunt, G. Ilsley, M. Kostadima, N. Langridge, J. E. Loveland, F. J. Martin, J. Morales, J. M. Mudge, M. Muffato, E. Perry, M. Ruffier, S. J. Trevanion, F. Cunningham, K. L. Howe, D. R. Zerbino, P. Flicek, Ensembl 2020. *Nucleic Acids Res.* **48**, D682–D688 (2020).
57. C. E. Grant, T. L. Bailey, W. S. Noble, FIMO: Scanning for occurrences of a given motif. *Bioinformatics* **27**, 1017–1018 (2011).
58. A. Shajahan, C. Heiss, M. Ishihara, P. Azadi, Glycomic and glycoproteomic analysis of glycoproteins—A tutorial. *Anal. Bioanal. Chem.* **409**, 4483–4505 (2017).
59. S. Oikari, T. Venäläinen, M. Tammi, Borate-aided anion exchange high-performance liquid chromatography of uridine diphosphate-sugars in brain, heart, adipose and liver tissues. *J. Chromatogr. A* **1323**, 82–86 (2014).

Acknowledgments: We thank W. Zhou and J. Liu in Anakk laboratory for the technical help. We are thankful to P. A.B. Orlean for the valuable feedback on glysolyation. We would like to thank the High-Throughput Sequencing Core and the Microscopy Core at UIUC. We would also like to thank the Comparative Biosciences Histology Laboratory for performing PAS staining and L. A. Miller from Material Sciences Laboratory for Electron microscopic analysis. We thank D. S. Rouhani for creating the art for the cover image. We thank D. Cromley and C. Vitali from Radar laboratory for expert technical assistance and helpful discussions. **Funding:** This research was supported through the Startup funds from University of Illinois at Urbana-Champaign, R01 DK113080 NIDDK; American Cancer Society grant RSG ACS132640 to S.A.; and in part through the NIH, National Glycoscience Resource, CCRC Service and Training (NIH grant no. R24GM137782-01) and the NIH–funded Orbitrap Fusion Tribrid Mass Spectrometer" (NIH grant no. 1S10OD018530) to P.A. Work in the Kalsotra laboratory is supported by the NIH (R01HL126845 and R01AA010154). Work in the Rader laboratory was supported by NIH grants HL134853, HL109489, and DK114291.
Author contributions: B.M. and S.A. conceived the project and designed the experiments. B.M., A.S., W.A., Q.C., N.J.H., L.K.A., and S.A. performed experiments and data analysis. K.S. shared the individual *Fxr*$^{fl/fl}$ and *Shp*$^{fl/fl}$ mice. B.M. generated the liver-specific *Fxr-Shp* knockout and control mice and characterized them. A.S., Q.C., and P.A. performed glycomics and glycoproteomics analyses. W.A. performed RNA-seq analysis. N.J.H. and D.J.R. generated and analyzed liver secretome plasma profiles. L.K.A. and J.A.H. quantitated the *O*-GlcNAc and hexosamine metabolites levels in the livers. B.M. and S.A. interpreted the results and wrote the manuscript. All authors discussed the results and edited the manuscript. **Competing interests:** The authors declare that they have no competing interests. **Data and materials availability:** All data needed to evaluate the conclusions in the paper are present in the paper and/or the Supplementary Materials. The RNA-seq data discussed in this publication have been deposited in NCBI's GEO (*55*) and are accessible through GEO Series accession number GSE164447 (www.ncbi.nlm.nih.gov/geo/query/acc.cgi?acc=GSE164447). Additional data related to this paper may be requested from the authors.

Submitted 30 October 2020
Accepted 4 March 2021
Published 21 April 2021
10.1126/sciadv.abf4865

Citation: B. Mathur, A. Shajahan, W. Arif, Q. Chen, N. J. Hand, L. K. Abramowitz, K. Schoonjans, D. J. Rader, A. Kalsotra, J. A. Hanover, P. Azadi, S. Anakk, Nuclear receptors FXR and SHP regulate protein N-glycan modifications in the liver. *Sci. Adv.* **7**, eabf4865 (2021).